



# TiN-contained polymer-metal core-shell structured nanocone array: Engineering of sensor performance by controlling plasmonic properties

Daiki Kawasaki<sup>a</sup>, Kenichi Maeno<sup>a</sup>, Hirotaka Yamada<sup>a</sup>, Kenji Sueyoshi<sup>a</sup>, Hideaki Hisamoto<sup>a</sup>, Tatsuro Endo<sup>a,b,\*</sup>

<sup>a</sup> Department of Applied Chemistry, Graduate School of Engineering, Osaka Prefecture University, Sakai 599-8531, Japan

<sup>b</sup> PRESTO, JST, Japan Science Technology Agency, 4-1-8 Honcho, Kawaguchi, Saitama 332-0012, Japan

## ARTICLE INFO

### Keywords:

Localized surface plasmon resonance (LSPR)  
Biosensor  
Titanium nitride  
Core-shell nanostructure  
Carrier engineering  
DNA detection

## ABSTRACT

Metal nanostructures have great potential for optical label-free biosensors based on localized surface plasmon resonance (LSPR). The sensitivity of a metal nanostructure-based label-free biosensor (i.e., plasmonic sensor) depends on its plasmonic properties, which suffer a decrease in sensitivity by energy losses in the metal material. Here, we demonstrate an approach to improve the plasmonic properties of metal nanostructures by controlling the carrier density in the base polymer material using titanium nitride (TiN). It is expected that the light energy absorbed by TiN is converted into excitons, and it will assist LSPs in the metal nanostructure; thus, the losses of the metal material are compensated by the excitons excited in TiN. We designed a TiN-contained polymer-metal/core-shell structured nanocone array (NCA), comprising TiN nanoparticles (NPs) in a polymer core and metal shell (Au or Ag), and realized improvement of the refractive index (RI) sensitivity of a label-free biosensor by optimizing the TiN-contained polymer composition. As a result, the TiN-contained polymer-metal NCA, with a TiN NP concentration of 10 wt% in the polymer core, had a 1.5-fold higher RI sensitivity than that of the same NCA without TiN NPs. The results of the resistance measurement of the metal surface with the TiN NP-contained polymer (10 wt%) under light exposure suggest the conversion of exposed light into LSPs of metal via TiN. It is suggested that plasmonic properties and sensor performances can be improved by the presented approach. Moreover, in DNA hybridization detection, an extremely low limit of detection of 117.5 fM was achieved.

## 1. Introduction

Metal nanostructures confine light in ultra-small volumes, beyond the diffraction limit, and convert light energy into localized surface plasmons (LSPs) by localized surface plasmon resonance (LSPR), significantly enhancing the localized electromagnetic (EM) field [1,2]. Localized EM field enhancement by metal nanostructures is a key phenomenon for optical sensing based on nanostructured materials, due to the potentials for manipulation of nanoparticles [3]; spontaneous emission enhancement, such as surface-enhanced Raman spectroscopy (SERS) [4]; and label-free sensing based on the surrounding refractive index (RI) change [5,6]. To realize a highly-sensitive plasmonic sensor, its localized EM field enhancement factor must be improved [7,8]. The localized EM field enhancement factor is related to the confinement efficiency of LSPs converted from light in a metal nanostructure, however, radiative and dissipative losses in metal nanostructures cause degradation of the confinement efficiency of LSPs [9,10]. Conventional approaches to reduce the energy losses in metal nanostructures are

often focused on structural shapes and sizes [11]. Edge-shaped metal nanostructures, such as nano prisms [12] and nano bowties [13], can efficiently confine LSPs to edge parts to create a strongly localized and highly enhanced EM field. Metal nanostructures with a nanogap can also strongly confine LSPs to the nanogap owing to the LSP interaction, i.e., the gap effect [14]. However, these structural approaches cannot solve the problem of the intrinsic losses of metal material. Meanwhile, improving the plasmonic property of metal material has great potential for developing highly-sensitive plasmonic sensors [15,16].

Recently, excitons in metal nanostructures excited by LSPR have attracted attention from various research fields, including photoelectric [17], photothermal [18], and photocatalytic research [19]. For photocatalysis, metal-semiconductor hybrid nanomaterials such as Ag-TiO<sub>2</sub> [20,21] and Au-ZnO [22,23] are widely studied. In this field, strongly confined light energy, as LSPs in metal nanostructures, is converted into exciton energy in a semiconductor [24]. LSP energy transfer to other elements, like dye molecules, is also applied in optical sensors using plasmon resonance energy transfer [25,26]. Many studies have reported

\* Corresponding author at: Department of Applied Chemistry, Graduate School of Engineering, Osaka Prefecture University, Sakai 599-8531, Japan.

E-mail address: [endo@chem.osakafu-u.ac.jp](mailto:endo@chem.osakafu-u.ac.jp) (T. Endo).

<https://doi.org/10.1016/j.snb.2019.126932>

Received 23 May 2019; Received in revised form 15 July 2019; Accepted 1 August 2019

Available online 04 August 2019

0925-4005/ © 2019 Elsevier B.V. All rights reserved.

the improvement of the performances of photo-induced functional devices using LSP energy conversion, and their conversion mechanisms, in detail [14,27–29]. However, these researches were focused on the energy conversion with the direction of LSPs to other elements via excitons. Meanwhile, it is well known that excitons in semiconductors with a higher energy than the Fermi level of metal can transfer to the neighboring metal [20,28], and those in semiconductor nanostructures can excite LSPs in themselves [30,31]. These phenomena suggest that excitons in a semiconductor can be converted, and they can assist LSPs in neighboring metal nanostructures. Focusing on this aspect, it is expected that the plasmonic properties of metal nanostructures can be improved by the exciton energy conversion into LSPs, and plasmonic sensor performances can be improved with a metal-semiconductor hybrid material.

Titanium nitride (TiN) is an alternative plasmonic material owing to its optical properties, easy fabrication, and cost being lower than that of noble metals such as gold and silver [32,33]. In addition, TiN nanostructures absorb light in the visible-NIR broadband region, and convert light into electrical and thermal energy with high efficiency [34]. Due to these excellent properties, TiN nanostructures have been applied in various fields including photothermal [35] and photocatalytic [36,37] devices, and plasmonic metamaterials [38,39].

We have developed a dielectric or metal nanostructure-based optical biosensor fabricated by nanoimprint lithography (NIL). We have achieved several successful optical biosensing results using nanostructure-based optical sensors [40–49]. Inside these sensors, the dielectric core-Au shell structured nanocone array (AuNCA) had a very high sensitivity for the label-free DNA sensor (LOD: 161 fM) [50]. AuNCA creates an enhanced EM field near its surface by LSPR in the visible region, increasing the RI sensitivity. However, the dissipative and radiative losses in the metal shell are relatively high compared with nano-edge or nanogap structures. The challenge to better the sensor performance of AuNCA is to improve its plasmonic properties by replacing the material with one that comprises AuNCA. Here, we designed a TiN-contained polymer-metal core-shell structured nanocone array (TiN-metal NCA) that comprises TiN nanoparticles (TiN NPs) contained within a polymer core and metal shell. By using TiN NPs, the optical property of a metal NCA can be controlled. In this study, a sufficiently high concentration of TiN NPs was used to prevent its own LSPR and to absorb the broadband of light efficiently. TiN NPs are expected to harvest light and convert it into LSPs in the metal shell efficiently, thus, improving the plasmonic properties of the metal shell. In this experiment, a TiN-metal NCA was fabricated by NIL [51] and its optical properties based on LSPR and RI sensitivity ( $S$  [nm/RIU]) [6,8] as the plasmonic sensor performance were evaluated. Au or Au/Ag was used as the metal material to fabricate the TiN-metal NCA here. To evaluate the conversion of the excitons excited by irradiated white light into the metal through the TiN NPs, TiN-metal sheets with the same TiN NP-contained polymer and metal compositions were independently fabricated, and the resistance of this hybrid material was systematically evaluated by varying the TiN NP concentration in the polymer. Finally, the correlation between the results of the resistance measurements and RI sensitivity of the TiN-metal NCA were fully evaluated in detail. Finally, label-free detection of DNA (ApoE) hybridization was performed and limit of detection was evaluated as a demonstration of the application of TiN-metal NCA for highly sensitive label-free biosensor (Fig. 1).

## 2. Material and methods

### 2.1. Fabrication of TiN-metal NCA

TiN NPs (diameter: 50 nm, Wako Pure Chem. Co., Osaka, Japan) were dispersed in acetone, then, the TiN-contained acetone was mixed with a photo-curable polymer (NOA81, Norland Products Inc, Cranbury, USA), followed by evaporation of the acetone. The

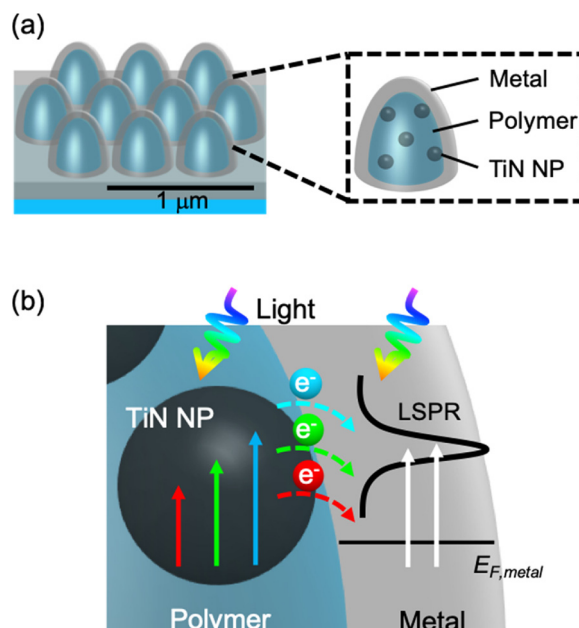


**Fig. 1.** Conceptual illustrations of TiN-metal NCA. (a) Schematic illustration of TiN-metal NCA. TiN-metal NCA consists of TiN NPs contained polymer core and metal layer shell. (b) Conceptual energy diagram applied to TiN-metal hybrid material. Exciton donation from TiN NPs to metal (dashed line) changes the plasmonic property.

concentrations of TiN NPs in the polymer were 0, 10, and 20 wt%. A TiN-contained polymer-metal NCA was fabricated by the NIL technique (Fig. 2). In this study, a moth-eye-structured Cyclo-olefin polymer (COP) film (FMES205/300-100 × 100, Scivax, Kawasaki, Japan) was used as the mold. The COP mold was cleaned by 2-propanol (KANTO CHEMICAL CO. Inc., Tokyo, Japan) and ultrapure water before drying at room temperature. A polyvinyl alcohol (PVA) (Wako Pure Chem. Co., Osaka, Japan) aqueous solution (20 wt%) was spin-coated at 4000 rpm on the COP mold and dried at 70 °C for 2 h. The PVA sacrificial mold was released and a metal layer (Au or Au/Ag) with a 50-nm thickness was thermally deposited onto the PVA sacrificial mold. Here, in the case of the NCA with a 50 nm-thick Au/Ag layer, the 10 nm Au layer was firstly deposited, followed by deposition of the 40 nm Ag layer onto the first Au layer, to avoid Ag layer oxidation while conducting measurements. The deposited metal layer was attached to the glass substrate by the TiN NP-contained photocurable polymer. Finally, followed by dissolving the PVA sacrificial mold in pure water, the TiN-metal NCA (NCA tips, 5 mm square) was obtained. Hereinafter, the TiN-contained polymer-metal NCA with the Au layer will be written as TiN-Au NCA and that with the Au/Ag layer as TiN-Ag NCA. The surface structures of the TiN-metal NCA were observed with field-emission scanning electron microscopy (FE-SEM) (SU8010, Hitachi, Ibaraki, Japan) at an acceleration voltage of 10 keV.

### 2.2. Sheet resistance measurement

The TiN-metal sheets with the same TiN-metal compositions were fabricated using the same fabrication process as that for the TiN-metal NCA, instead using a COP film with a flat surface as the mold. The sheet resistance ( $\rho$  [mΩ]) was measured by a four-point probe (Asratec Co., Tokyo, Japan.). To avoid contact resistance in the four-point probe measurement, a constant current was applied to two probes and the potential on the other two probes was measured with a resistance meter (HIOKI E.E. Co. Nagano, Japan). The sample sheet was set on the stage of an inverted microscope, then the sheet resistance of the sample exposed ( $\rho$  (on)) or unexposed ( $\rho$  (off)) to white light by a UV lamp (wavelength: 200 ~ 600 nm, OLYMPUS, U-RFL-T, Tokyo, Japan) was

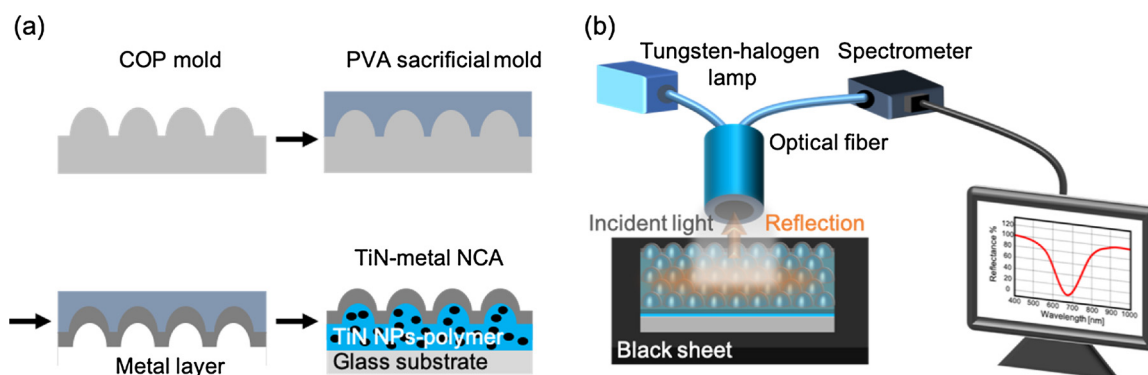


**Fig. 2.** Experimental method schematic: (a) Nanoimprint lithography fabrication process of the TiN-metal NCA. A 50-nm thick Au or 10/40-nm thick Au/Ag layer was deposited as the metal layer. (b) Schematic of the optical setup in this study. A black sheet was placed under the NCA sample to absorb transmitted light. The reflectance spectra were measured and the subtracted spectrum  $1-R$  was calculated.

measured. Sheet resistance measurements were performed in triplicates using three independent samples ( $N = 3$ ).

### 2.3. Optical characterization

The optical setup comprised of a tungsten halogen light source (LS-1), a fiber probe (R400-7, UV-VIS), a spectrophotometer (USB4000), and software (Ocean View), all purchased from Ocean Optics, Tokyo, Japan. The reflection spectra of the NCAs were measured, and the absorption spectra ( $1-R$ ) were calculated. We used flat sheets with the same composition of TiN-metal NCA (TiN-metal sheet) as that in the reference samples for the measurement. Mixed solutions of 2-propanol and pure water (1:1, 1:3, 0:1; RI:  $n = 1.3329, 1.3590, 1.3757$ , respectively) were prepared and used for the measurement of the RI sensitivities of the TiN-metal NCA samples. Triplicate optical measurements were performed using three independent NCA tips ( $N = 3$ ). A finite difference time domain method-based solution (Lumelical Solutions, Inc., Vancouver, Canada) was used as the software for calculation. The simulated model was constructed based on the AFM image of the moth-eye-structured COP mold (Figs. S1 and S2).

### 2.4. Label-free detection of DNA hybridization

In this study, TiN-Au NCA (TiN NPs: 10 wt%) was applied for label-free detection of DNA hybridization. The oligonucleotides used in the present study are following. They were purchased from BEX Co. Ltd. (Toyota, Japan). 5' disulfide-modified 23 base pair (bp) long sequence probe and fully complementary target DNA were used in the present study. A buffer solution (pH 7.4) containing NaCl (300 mM),  $\text{Na}_2\text{HPO}_4 \cdot 12\text{H}_2\text{O}$  (20 mM), and EDTA (0.1 mM), all purchased from Wako Pure Chem. Co. (Osaka, Japan), was used to immobilize the thiolated probe onto Au surface and the hybridization of the target DNA. The thiolated probe DNA (100 nM in buffer) was immobilized on the TiN-Au NCA surface by incubating at 37 °C for overnight, then immersing in ultrapure water for 1 h to remove non-specifically adsorbed DNA and buffer solution. Complementary target DNA (1 fM to 1 nM in buffer) was hybridized by incubating at 37 °C for 1 h, and then immersing in ultrapure water for 30 min, followed by drying at room temperature. Optical measurements were performed by reflection spectroscopy. The peak shifts for each DNA samples were analyzed. Triplicate optical measurements for all DNA samples were performed using three independent TiN-Au NCA samples ( $n = 3$ ). In this experiment, we used DNase-free water (Table 1).

**Table 1**

Oligonucleotides sequences\* studied in this report.

	Sequence (5' to 3')
Probe DNA	HS-ACCTGCAGAAGCGCTGGCAGTG
Complementary DNA	CACTGCCAGGCGCTTCTGCAGGT

## 3. Results and discussion

### 3.1. Fabrication of TiN-metal NCA

The fabricated NCA (TiN NPs: 10 wt%) without a metal layer is shown in Fig. 3(a). It absorbed white light well and became black in color. No modification of the TiN NPs was made and the ease of the preparation process of the TiN-contained polymer enabled the TiN-metal NCA to be fabricated simply and speedily. While the NCA without a metal layer (TiN NPs: 10 wt%) colored black, the TiN-metal NCA with the Au/Ag layer (TiN NPs: 10 wt%) colored yellow due to LSPR in the metal layer (Fig. 3(b)). The surface structure of the TiN-metal NCA matched well with the original surface of the moth-eye-structured mold (Fig. S1), thus a TiN-metal NCA with few defects was fabricated successfully using the NIL process.

### 3.2. Photoelectrical characterization of TiN-metal sheet

The TiN-metal sheet resistance change associated with light irradiation was investigated (Fig. 4(a) and (b)). The results showed that the sheet resistance decreased with the increment of TiN NP concentration, while the sheet resistance values of the TiN-Ag and TiN-Au sheets were different due to the difference in the resistance between Au and Ag. The decrement of  $\rho$  (off) indicates that carriers in the TiN-metal sheet increased due to the carriers in the TiN NPs located near the metal layer. The sheet resistances of the TiN-metal sheets with different concentrations of TiN NPs were changed by light irradiation. The error bar of the sheet resistance might indicate error in the dispersiveness of the TiN NPs in the polymer. The TiN NPs located near the interface of the polymer and metal layer were assumed to effect the electrical property of the metal layer more than that of those located far from the interface because the electrons in the TiN NPs on or near the interface, within a few nanometers, can transfer to the metal layer. The number of TiN NPs near the interface was expected to be generally proportional to the concentration of TiN NPs. Hence, we focused on the relationship between the electrical property of the TiN-metal sheet and the concentration of TiN NPs in the polymer. Then, the ratio of the reciprocal of resistance (conductivity)  $\rho^{-1}$  with light irradiation ( $\rho^{-1}(\text{on})$ ) to that without light irradiation ( $\rho^{-1}(\text{off})$ ), defined as a factor:  $f = \rho^{-1}(\text{on}) / \rho^{-1}(\text{off})$ , was calculated (Fig. 4(c)). In the case of 0 wt% concentration

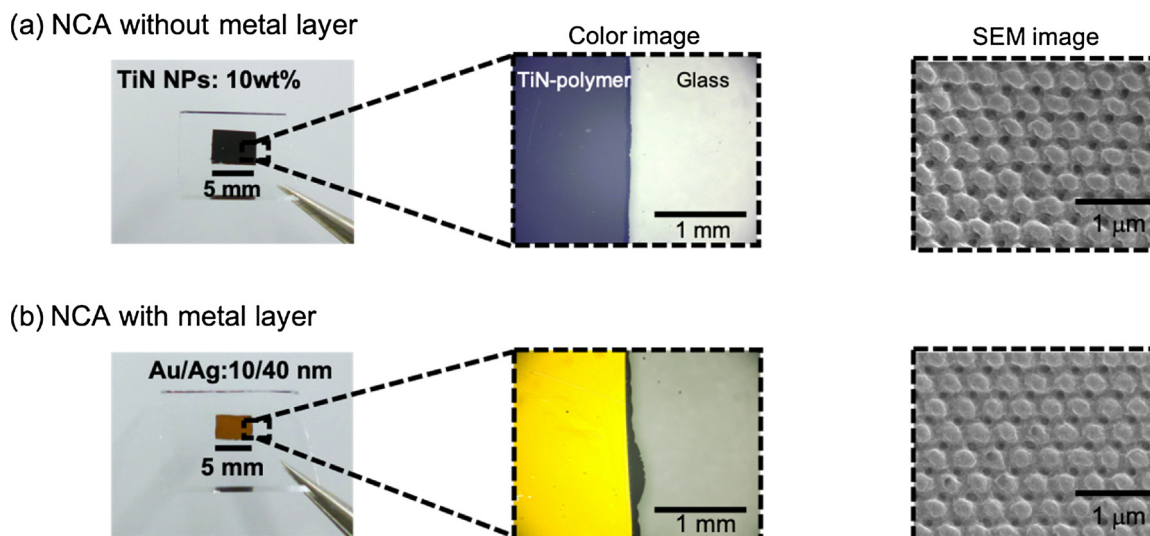


**Fig. 3.** Images of NCA chips (left), the NCA color as observed by a digital microscope and its surface structure as observed by FE-SEM (right) with and without a metal layer. (a) Images of NCA comprising TiN NP-contained (10 wt%) polymer core without a metal layer. As shown, the NCA core absorbs light and colored black. To clearly observe the NCA surface structure by SEM, Pt nanoparticles were sputtered on the surface. (b) Images of TiN-Ag NCA; with the metal layer, the NCA colored due to LSPR.

of TiN NPs,  $f_{Ag}$  was almost 1 because the absorption cross-section of Ag is small, thus, the electric loss caused by light irradiation was too small to change the resistance. In contrast,  $f_{Au}$  was less than 1 because the absorption cross-section of Au is large enough to increase the resistance due to light absorption. The notable point is that  $f$  exhibited its maximum value at 10 wt% concentration of TiN NPs for both the Au and Ag layers, and was lower at the 20 wt% and 0 wt% concentrations. This result indicates that the apparent dielectric losses in the metal reduced at 10 wt% TiN NPs while they increased at 20 wt%. It was suggested that the generated excitons in TiN due to light absorption transferred to the metal layer and simultaneously served as carriers of the energy loss in TiN. For 10 wt% concentration of TiN NPs, the effect of the former was likely to be larger than the latter and vice versa in the cases of 20 wt% and 0 wt%. These results also suggest that the excitons generated in TiN were converted into LSPs in the metal layer. Considering the TiN-metal hybrid material, and that the effect of the energy loss in TiN is larger than the effect of the energy conversion, LSPs in the metal layer would decrease due to the energy loss in TiN. Thus, the resistance change caused by light irradiation, as shown in Fig. 4, is regarded to be mainly associated with the energy loss in TiN of the TiN-metal hybrid material; this is also an important factor for the RI sensitivity of the TiN-metal NCA. However, the carrier density increments by the TiN NPs

contained in the core should also be considered for the TiN-metal NCA because they effect the LSP properties, such as the blue-shift of the LSPR excitation wavelength. It is assumed that the plasmonic properties of the TiN-Ag NCA depend largely on the loss in TiN because Ag has a much smaller damping, while that of the Au-metal hybrid material depends less on TiN because Au has a higher energy loss than Ag. Hence, the metal layer material plays a prominent role in the excitation of LSPR, while TiN could assist LSPs in the metal layer due to the generation of excitons in TiN by light absorption.

### 3.3. Optical characterization of TiN-metal NCA

The TiN-metal NCA absorbs light of a specific wavelength due to LSPR excitation in the metal layer. The LSPR excitation wavelength depends on various factors, such as the size and form of the nanostructure, and the surrounding dielectric constant and electric property of the material. We investigated the correlation between the LSPR excitation wavelength and the TiN NP concentration in the TiN-metal NCA. Additionally, the sheet resistance of the TiN-metal sheet under white light exposure was measured to evaluate the correlation between the LSPR excitation wavelength of the TiN-metal NCA, as well as that of the corresponding TiN-metal sheet. The absorption spectra of the TiN-

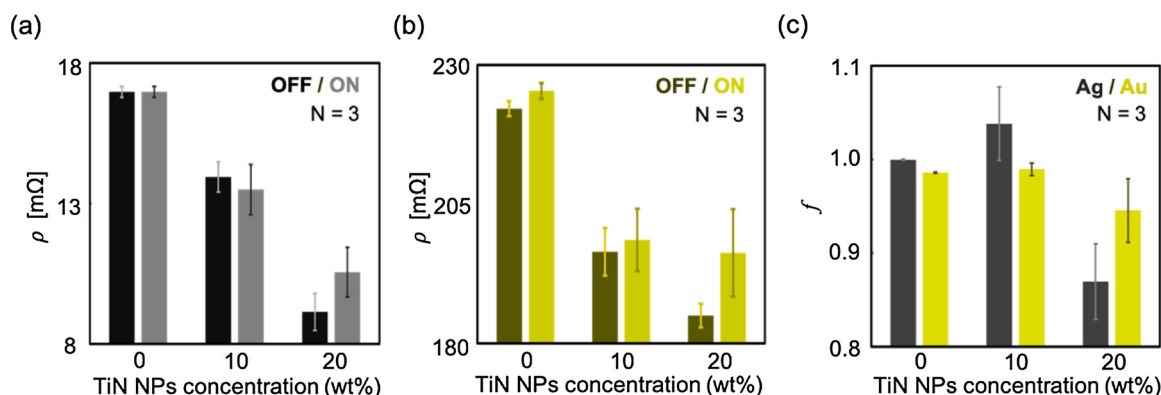


**Fig. 4.** Sheet resistance measurements of (a) TiN-Au and (b) TiN-Ag sheets under light exposure and non-exposure. The sheet resistance changed by the light irradiation to the TiN metal sheet, and decreased with the increment of the TiN NP concentration. (c) Ratio of conductance under light exposure ( $\rho^{-1}$  (on)) and non-exposure ( $\rho^{-1}$  (off)), defined as  $f = \rho^{-1}(\text{on}) / \rho^{-1}(\text{off})$ . The rate of increment of the conductance due to light irradiation exhibited its maximum value at 10 wt% concentration of TiN NPs. Three independent sample surfaces were measured ( $N = 3$ ).



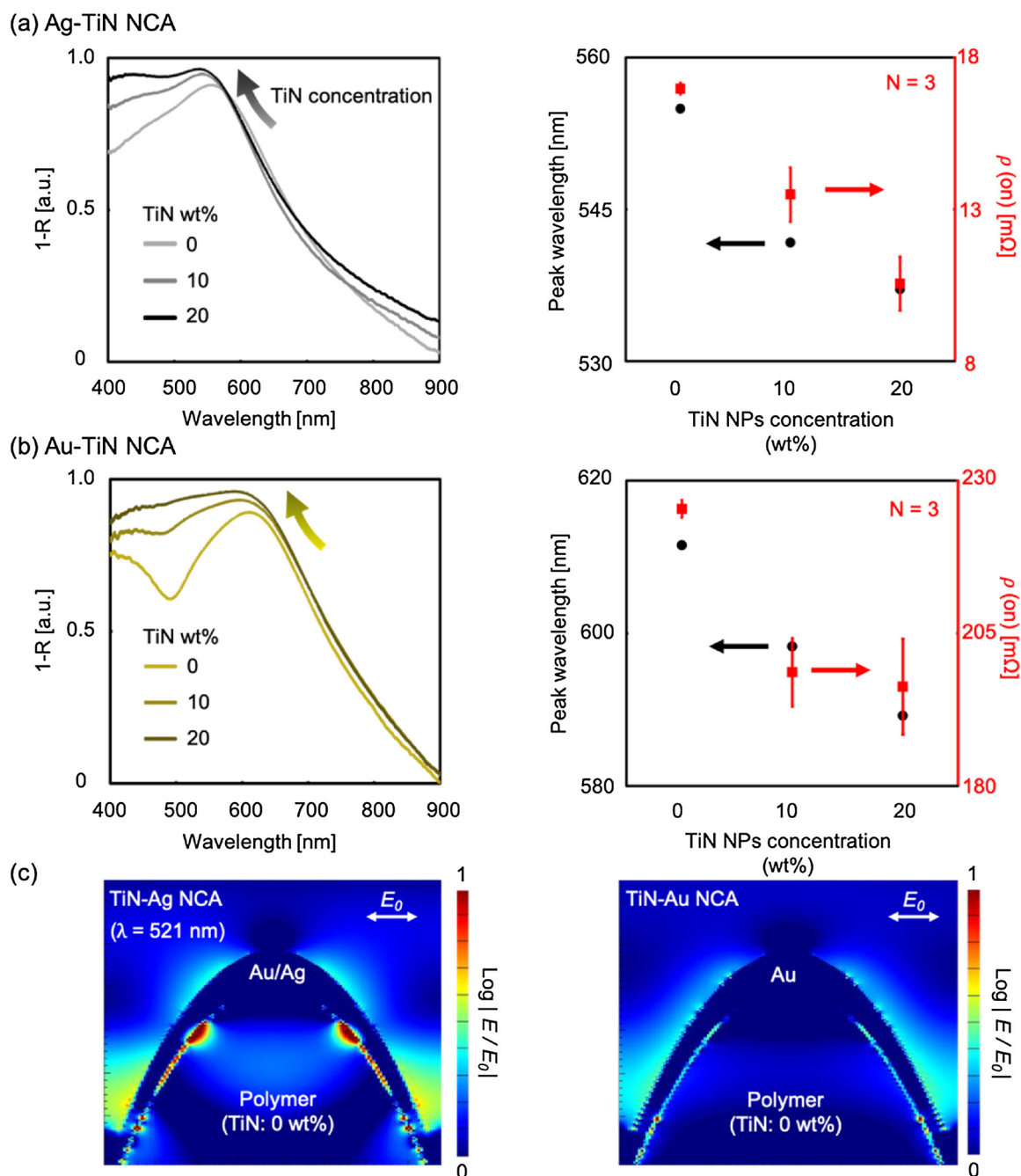


**Fig. 5.** Optical property of the TiN-metal NCA characterized by the measurement of the absorption (1-R) spectrum of the TiN-metal NCA and the TiN-metal sheet resistance. (a) Absorption spectra of the TiN-Ag NCA (left) indicating the increment of the absorption intensity and the blue-shift of the LSPR-induced absorption peak wavelength with the increment of TiN NP concentration. A plot of the absorption peak wavelength and sheet resistance under whitelight exposure ( $\rho$  (on)) to TiN NP concentration is also shown (right). The absorption peak wavelength blue-shifted with the sheet resistance decrement. (b) The same tendency was confirmed for the TiN-Au NCA as for the TiN-Ag NCA, though their peak wavelengths and sheet resistances are different due to the difference in their electrical properties. (c) Enhanced electric field distribution created by the NCA without TiN NPs (i.e., TiN: 0 wt%) at the simulated absorption peak wavelength (TiN-Ag: 521 nm, TiN-Au: 597 nm), indicating that the absorption in these spectra are attributed to LSPR excitation.

Ag NCA are shown in Fig. 5(a). The absorption intensity increased and the wavelength of the absorption peak induced by LSPR excitation blue-shifted with the increase of TiN NP concentration in the NCA core. The increment of the absorption intensity resulted from the absorption by the TiN NPs. Fig. 5 shows plots of the peak wavelength and sheet resistance under white light exposure ( $\rho$  (on)), as shown in Fig. 4(a) and (b), against the TiN NP concentration in the polymer. It was confirmed that the blue-shift of the peak wavelength correlates with the decrement of the sheet resistance. This result suggests that the LSPR excitation wavelength was blue-shifted due to the resistance decrease and

agrees with the blue-shift of the LSPR excitation wavelength with the increment of the carrier density in the metal material. The same tendency of the optical property change to TiN concentration of the TiN-Ag NCA was confirmed in the case of the TiN-Au NCA, though the LSPR excitation wavelength and sheet resistance value were different from the TiN-Ag NCA due to the difference in the electrical property between Au and Ag (Fig. 5(a) and (b)). The electromagnetic field simulation (Fig. S3) indicated that the absorption in the experimental spectra was caused by LSPR in the metal layer. As shown in Fig. 5(c), an enhanced EM field was created near the outer surface of the NCA at the simulated

absorption peak wavelength (Fig. S4) and the enhanced EM field distribution in the outer surface of the Ag NCA was similar to that of Au NCA. These results suggest that the LSPR property of the TiN-metal NCA depends on TiN NP concentration in the core and that the sensor performance of the TiN-metal NCA correlates with TiN NP concentration. Additionally, the EM field enhancement factor  $|E/E_0|$  of the Ag NCA was higher than that of the Au NCA because Ag has better electrical properties for LSPR excitation, such as lower damping and a higher carrier density, than Au. Thus, the loss of LSPs in the Ag NCA was lower than in the Au NCA, hence, the Ag NCA has a higher potential for developing highly-sensitive sensors than Au NCA.

### 3.4. Sensor performance characterization of TiN-metal NCA

The LSPR excitation wavelength depends on the RI of the medium surrounding the metal nanostructure. Generally, the LSPR excitation wavelength red-shifts with the increment of the RI near a metal nanostructure [6]. This property of LSPR is applied to the label-free detection of biomolecular events, such as antigen-antibody interaction, DNA hybridization, and DNA-protein interaction. Thus, the RI sensitivity ( $S = \delta\lambda/\delta n$  [nm/RIU]) of a metal nanostructure is an important factor for LSPR-based sensors. In this section, the correlation between the RI sensitivity of the TiN-metal NCA and the TiN NP concentration in the polymer core are evaluated. The absorption spectra of the TiN-metal NCA with 10 wt% concentration of TiN NPs in mixed solutions of water and IPA are shown in Fig. 6(a) and (b), and the simulated absorption spectra of the NCA without TiN in water are shown in Fig. S5. The simulated absorption spectra exhibit two distinct absorption peaks. Based on the simulation of the enhanced EM field distribution, it was observed that LSPR of a shorter wavelength was attributed to the

interface between the polymer core and the metal layer, and that of a longer wavelength was attributed to the outside surface of the metal layer. Thus, the latter mode is considered to contribute to RI sensitivity. In the experiment, the absorption peak of the longer wavelength red-shifted with the increment of the solution's RI. The RI sensitivity  $S$  was then calculated based on the slope of the calibration line, shown as the peak wavelength shift to the RI in Fig. 6(c). The peak wavelength shift is defined as the wavelength shift from the peak wavelength of the background signal (aqueous solution: RI = 1.3329) to that for the sample solution of a higher RI. The RI sensitivity of the TiN-metal NCA exhibited its maximum value at 10 wt% concentration of TiN NPs (approximately 1.5-fold increase from the NCA without TiN NPs) regardless of metal material. Additionally, as expected, the RI sensitivity of the Ag NCA was higher than that of the Au NCA (Fig. 6(c)) due to the higher EM field enhancement factor of Ag than that of Au, as shown in Fig. 5(c). Comparing the RI sensitivity change (Fig. 6(d)) and  $f$  (Fig. 4(c)), in the case of Ag,  $f_{Ag}$  contributes largely to the RI sensitivity because the fluctuation of the RI sensitivity agrees with  $f_{Ag}$ , while in the case of Au, the carrier density change was also considered to contribute largely to the RI sensitivity because the fluctuation of the RI sensitivity differed from  $f_{Au}$ . These results indicate that the excitons generated in the TiN NPs could assist LSPs in the metal layer, thus improving the sensor performance of the NCA by the TiN-metal hybrid material with less losses than a metal material, which would be applied to other plasmonic sensors.

### 3.5. Label-free detection of DNA hybridization

TiN-Au NCA with 10 wt% concentration of TiN NPs was used for the detection of DNA hybridization. The probe DNA immobilization to TiN-

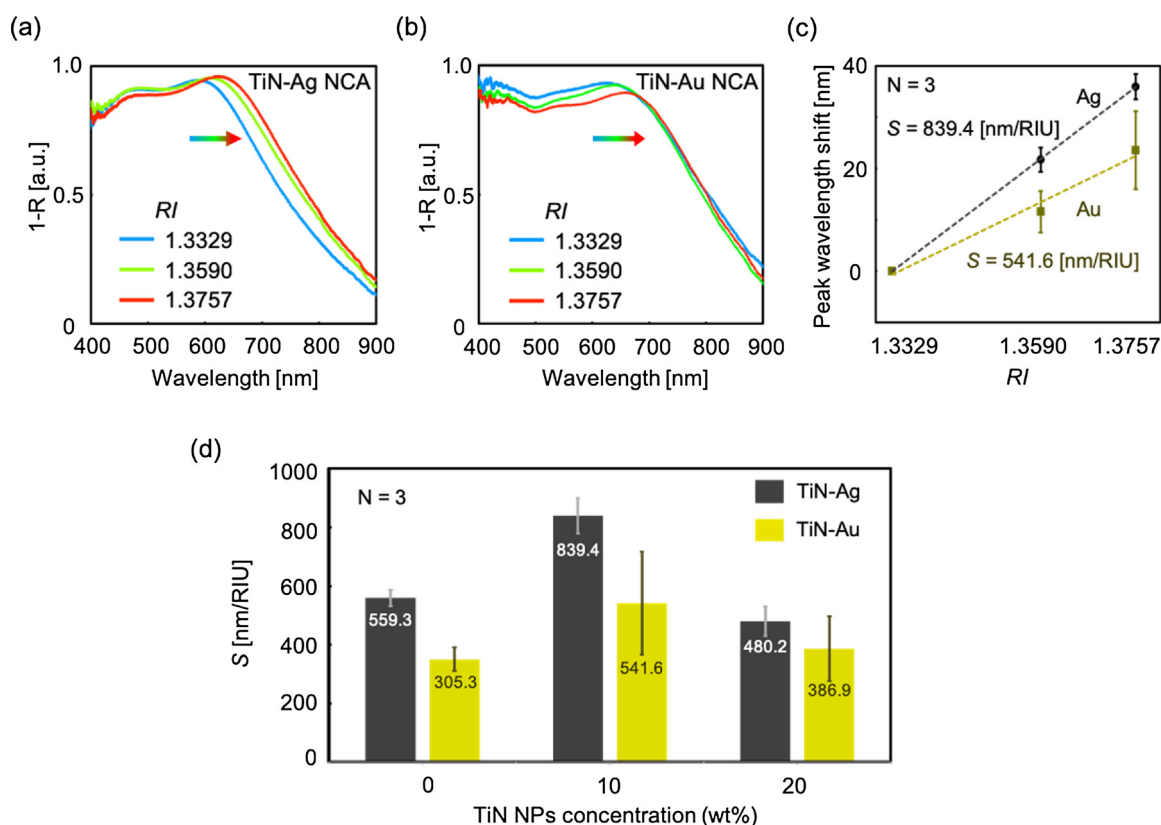


**Fig. 6.** Evaluation of the RI sensitivity of the TiN-metal NCA. Absorption spectra of (a) TiN-Ag NCA and (b) TiN-Au NCA with 10 wt% concentration of TiN NPs in solutions of water and IPA with different RI values. The absorption peak wavelength red-shifted as the RI increased. (c) Plots of the absorption peak wavelength shifts to the RI values in (a) and (b) and the RI sensitivities based on the slope of the calibration line. (d) Plot of the RI sensitivity of TiN-Ag and Au NCA against TiN NP concentration. The averaged RI sensitivity value is described by the bar. The RI sensitivity was highest at 10 wt% concentration of TiN NPs. Three independent TiN-metal NCA samples were used ( $N = 3$ ).

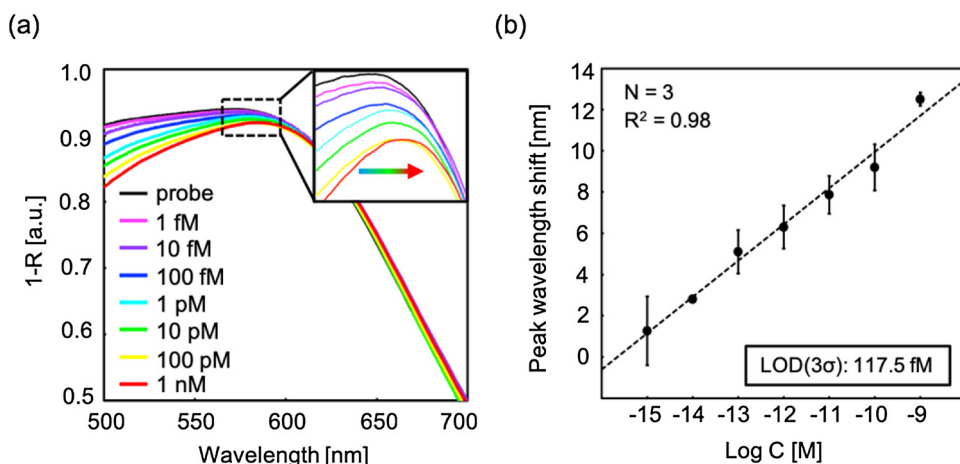


**Fig. 7.** DNA hybridization detection by TiN-Au NCA with 10 wt% concentration of TiN NPs (a) Absorption spectra of TiN-Au NCA after immobilization of probe DNA (black), and after hybridization of each concentration of target DNA (colored). (b) Calibration curve of hybridization detection of target DNA. Peak shift was defined as the wavelength shift from the peak wavelength of probe immobilized TiN-Au NCA. Limit of detection ( $3\sigma$ ) was 117.5 fM.

Au NCA was confirmed by the absorption peak wavelength shift of  $6.5 \pm 0.8$  nm ( $n = 3$ ) (Fig. S5). Complementary DNAs were detected based on the absorption peak wavelength shift from that of the probe DNA immobilized TiN-Au NCA. The quantitative determination of the complementary DNA was performed in a concentration range from 1 fM to 1 nM. As the complementary DNA was hybridized to probe DNA on TiN-Au NCA, the peak wavelength was red-shifted (Fig. 7a). Then, the calibration curve was obtained ( $n = 3$ ) (Fig. 7b). The calibration curve had linearity and a limit of detection ( $3\sigma$ ) of TiN-Au NCA (TiN NPs: 10 wt%) was determined to be 117.5 fM, which is a lower value than that of AuNCA in our previous study. Moreover, the optimization of the thickness of Au layer will improve the sensitivity of TiN-Au NCA. In previous study, the absorption intensity was increased with the red-shift of the peak wavelength in the detection of DNA hybridization [50], however, as shown in Fig. 7a, the absorption intensity decreased with the red-shift of the peak wavelength. The absorption intensity at the wavelength range from 500 nm to 600 nm was decreased as the concentration of complementary DNA was increased. This result suggested that the light absorption by TiN NPs in polymer core was decreased and electron transition from TiN NPs to Au layer at the interface was reduced as the adsorbed DNA molecules on the outside surface of TiN-Au NCA were increased. Then, the decrement of carrier density as well as the increment of refractive index surrounding outside surface could red-shifts the peak wavelength. In order to reveal the mechanism of this results, more detailed electronic properties have to be investigated. Here, complementary DNAs were also detected based on the absorption peak intensity change from that of the probe DNA immobilized TiN-Au NCA. Then, the calibration curve was obtained ( $n = 3$ ). This calibration curve also had linearity and a limit of detection ( $3\sigma$ ) was 14.5 fM (Fig. S6). This calibration curve also had linearity and a limit of detection ( $3\sigma$ ) was 14.5 fM (Fig. S6). This detection limit is better than the method using plasmonic nanostructure [52], and is as low as the electronic nanosensor using silicon nanowire [53].

#### 4. Conclusions

In this report, we demonstrated the improvement of plasmonic sensor performance by designing a TiN-metal hybrid material. The present approach improved the efficiency of the light energy concentration and conversion into LSPs in the metal nanostructure. We applied this hybrid material to a core-shell structured NCA, which potentially has a high RI sensitivity due to the NCA's ability to create an extensively enhanced EM field near its surface. Easy and high-throughput fabrication of the TiN-metal NCA was achieved using the NIL technique. The resistance of the TiN-metal hybrid material decreased as the concentration of TiN NPs increased, even in the dark condition. Furthermore, as the resistance decreased, the LSPR

wavelength blue-shifted. The RI sensitivity of the TiN-metal NCA exhibited its maximum value at 10 wt% concentration of TiN NPs in the polymer core, being approximately 1.5-fold higher than the polymer-metal NCA without TiN NPs. Additionally, the decrement of the resistance due to light absorption was inhibited the most at the same concentration (10 wt%) of TiN NPs in the polymer. Based on these results, it was suggested that excitons generated in TiN transferred to the metal, improving the plasmonic properties of the metal. In the application of TiN-Au NCA (TiN NPs: 10 wt%) to the detection of DNA hybridization, extremely highly sensitive detection with the limit of detection ( $3\sigma$ ) of 117.5 fM was successfully achieved. Moreover, DNA hybridization was detected not only by the absorption peak shift but also peak intensity change, which was decreased as the concentration of complementary DNA to be detected was increased contrary to the peak intensity increment in previous work. It was expected that TiN NPs had some effects on the peak wavelength shift and the intensity change in detection of DNA hybridization. In this study, we applied TiN to the hybrid material because it has enough rich carriers to absorb light well. Other materials that suffer fewer losses and are richer in carriers than TiN, for example, ZrN, would be a suitable alternative to the present approach [39]. We have proposed one approach to improve the plasmonic properties in a metal nanostructure, which will open the way for further improvements to the sensitivity of plasmonic sensors based on metal nanostructures.

#### Appendix A. Supplementary data

Supplementary material related to this article can be found, in the online version, at doi:<https://doi.org/10.1016/j.snb.2019.126932>.

#### References

- [1] B.S.A. Maier, M.L. Brongersma, P.G. Kik, S. Meltzer, A.A.G. Requicha, H.A. Atwater, Plasmonics—A route to nanoscale optical devices, *Adv. Mater.* 13 (2001) 1501–1505.
- [2] J.A. Schuller, E.S. Barnard, W. Cai, Y.C. Jun, J. White, Mark L. Brongersma, Plasmonics for extreme light concentration and manipulation, *Nat. Mater.* 9 (2010) 193–204.
- [3] M. Righini, G. Volpe, C. Girard, D. Petrov, R. Quidant, Surface plasmon optical tweezers: tunable optical manipulation in the femtonewton range, *Phys. Rev. Lett.* 100 (2008) 8–11.
- [4] C. Zong, M. Xu, L. Xu, T. Wei, X. Ma, X. Zheng, R. Hu, B. Ren, Surface-enhanced Raman spectroscopy for bioanalysis: reliability and challenges, *Chem. Rev.* 118 (2018) 4946–4980.
- [5] J. Jatschka, A. Dathe, A. Csáki, W. Fritzsche, O. Stranik, Propagating and localized surface plasmon resonance sensing — A critical comparison based on measurements and theory, *Sens. Bio Sens. Res.* 7 (2016) 62–70.
- [6] T. Chung, S. Lee, E.Y. Song, H. Chun, B. Lee, Plasmonic nanostructures for nanoscale bio-sensing, *Sensors* 11 (2011) 10907–10929.
- [7] K.S. Lee, M.A. El-Sayed, Gold and silver nanoparticles in sensing and imaging: sensitivity of plasmon response to size, shape, and metal composition, *J. Phys. Chem. B* 110 (2006) 19220–19225.

- [8] M.M. Miller, A.A. Lazarides, Sensitivity of metal nanoparticle surface plasmon resonance to the dielectric environment, *J. Phys. Chem. B* 109 (2005) 21556–21565.
- [9] G.V. Hartland, Optical studies of dynamics in noble metal nanostructures, *Chem. Rev.* 111 (2011) 3858–3887.
- [10] P. Mulvaney, Surface plasmon spectroscopy of nanosized metal particles, *Langmuir* 12 (1996) 788–800.
- [11] K.L. Kelly, E. Coronado, L.L. Zhao, G.C. Schatz, The optical properties of metal nanoparticles: the influence of size, shape, and dielectric environment, *J. Phys. Chem. B* 107 (2003) 668–677.
- [12] L.J. Sherry, R. Jin, C.A. Mirkin, G.C. Schatz, R.P. Van Duyne, Localized surface plasmon resonance spectroscopy of single silver triangular nanoprisms, *Nano Lett.* 6 (2006) 2060–2065.
- [13] B.J. Roxworthy, K.D. Ko, A. Kumar, K.H. Fung, E.K.C. Chow, G.L. Liu, N.X. Fang, K.C. Toussaint, Application of plasmonic bowtie nanoantenna arrays for optical trapping, stacking, and sorting, *Nano Lett.* 12 (2012) 796–801.
- [14] J. Cuadra, D.G. Baranov, M. Wersäll, R. Verre, T.J. Antosiewicz, T. Shegai, Observation of tunable charged exciton polaritons in hybrid monolayer WS<sub>2</sub>-plasmonic nanoantenna system, *Nano Lett.* 18 (2018) 1777–1785.
- [15] P.R. West, S. Ishii, G.V. Naik, N.K. Emani, V.M. Shalae, Searching for better plasmonic materials, *Laser Photon. Rev.* 4 (2010) 795–808.
- [16] B. Doiron, M. Mota, M.P. Wells, R. Bower, A. Mihai, Y. Li, L.F. Cohen, N.M. Alford, P.K. Petrov, R.F. Oulton, S.A. Maier, Quantifying figures of merit for localized surface plasmon resonance applications: a materials survey, *ACS Photonics* 10 (2019) 1–20.
- [17] X. Li, C. Jia, B. Ma, W. Wang, Z. Fang, G. Zhang, X. Guo, Substrate-induced interfacial plasmonics for photovoltaic conversion, *Sci. Rep.* 5 (2015) 14497.
- [18] X. Huang, P.K. Jain, I.H. El-Sayed, M.A. El-Sayed, Plasmonic photothermal therapy (PPTT) using gold nanoparticles, *Lasers Med. Sci.* 23 (2008) 217–228.
- [19] Y. Zhang, S. He, W. Guo, Y. Hu, J. Huang, J.R. Mulcahy, W.D. Wei, Surface-plasmon-driven hot electron photochemistry, *Chem. Rev.* 118 (2018) 2927–2954.
- [20] A. Takai, P.V. Kamat, Capture, store, and discharge. Shuttling photogenerated electrons across TiO<sub>2</sub>-silver interface, *ACS Nano* 5 (2011) 7369–7376.
- [21] S. Tan, A. Argondizzo, J. Ren, L. Liu, J. Zhao, H. Petek, Plasmonic coupling at a metal/semiconductor interface, *Nat. Photonics* 11 (2017) 806–813.
- [22] W.H. Lin, Y.H. Chiu, P.W. Shao, Y.J. Hsu, Metal-particle-decorated ZnO nanocrystals: photocatalysis and charge dynamics, *ACS Appl. Mater. Interfaces* 8 (2016) 32754–32763.
- [23] W. He, H.K. Kim, W.G. Wamer, D. Melka, J.H. Callahan, J.J. Yin, Photogenerated charge carriers and reactive oxygen species in ZnO/Au hybrid nanostructures with enhanced photocatalytic and antibacterial activity, *J. Am. Chem. Soc.* 136 (2014) 750–757.
- [24] N. Wu, Plasmonic metal-semiconductor photocatalysts and photoelectrochemical cells: a review, *Nanoscale* 10 (2018) 2679–2696.
- [25] T. Kang, L.P. Lee, Y. Choi, Plasmon resonance energy transfer (PRET)-based molecular imaging of cytochrome c in living cells, *Nano Lett.* 9 (2009) 85–90.
- [26] L. Shi, C. Jing, Z. Gu, Y.T. Long, Brightening gold nanoparticles: new sensing approach based on plasmon resonance energy transfer, *Sci. Rep.* 5 (2015) 10142.
- [27] M.J. Kale, T. Avanesian, P. Christopher, Direct photocatalysis by plasmonic nanostructures, *ACS Catal.* 4 (2014) 116–128.
- [28] S.H. Lee, S.W. Lee, T. Oh, S.H. Petrosko, C.A. Mirkin, J.W. Jang, Direct observation of plasmon-induced interfacial charge separation in Metal/Semiconductor hybrid nanostructures by measuring surface potentials, *Nano Lett.* 18 (2018) 109–116.
- [29] M.L. Brongersma, N.J. Halas, P. Nordlander, Plasmon-induced hot carrier science and technology, *Nat. Nanotechnol.* 10 (2015) 25–34.
- [30] J.A. Fauchaux, A.L.D. Stanton, P.K. Jain, Plasmon resonances of semiconductor nanocrystals: physical principles and new opportunities, *J. Phys. Chem. Lett.* 5 (2014) 976–985.
- [31] A. Agrawal, S.H. Cho, O. Zandi, S. Ghosh, R.W. Johns, D.J. Milliron, Localized surface plasmon resonance in semiconductor nanocrystals, *Chem. Rev.* 118 (2018) 3121–3207.
- [32] D. Jang, L.R. Meza, F. Greer, J.R. Greer, Fabrication and deformation of three-dimensional hollow ceramic nanostructures Dongchan, *Nat. Mater.* 12 (2013) 893–898.
- [33] T. Wood, M. Naffouti, J. Berthelot, T. David, J.-B. Claude, L. Métayer, A. Delobbe, L. Favre, A. Ronda, I. Berbezier, N. Bonod, M. Abbarchi, All-dielectric color filters using SiGe-based Mie resonator arrays, *ACS Photonics* 4 (2017) 873–883.
- [34] P. Patsalas, N. Kalfagiannis, S. Kassaveti, Optical properties and plasmonic performance of titanium nitride, *Materials* 8 (2015) 3128–3154.
- [35] U. Guler, J.C. Ndukaife, G.V. Naik, A.G.A. Nnanna, A.V. Kildishev, V.M. Shalae, A. Boltasseva, Local heating with lithographically fabricated plasmonic titanium nitride nanoparticles, *Nano Lett.* 13 (2013) 6078–6083.
- [36] S. Rtimi, O. Baghrich, R. Sanjines, C. Pulgarin, M. Ben-Simon, J.C. Lavanchy, A. Houas, J. Kiwi, Photocatalysis/catalysis by innovative TiN and TiN-Ag surfaces inactivate bacteria under visible light, *Appl. Catal. B Environ.* 123–124 (2012) 306–315.
- [37] A. Naldoni, U. Guler, Z. Wang, M. Marelly, F. Malara, X. Meng, L.V. Besteiro, A.O. Govorov, A.V. Kildishev, A. Boltasseva, V.M. Shalae, Broadband hot-electron collection for solar water splitting with plasmonic titanium nitride, *Adv. Opt. Mater.* 5 (2017) 1601031.
- [38] W. Li, U. Guler, N. Kinsey, G.V. Naik, A. Boltasseva, J. Guan, V.M. Shalae, A.V. Kildishev, Refractory plasmonics with titanium nitride: broadband, *Adv. Mater.* 26 (2014) 7959–7965.
- [39] U. Guler, A. Boltasseva, V.M. Shalae, Refractory plasmonics, *Science* (80-) 344 (2014) 263–264.
- [40] S. Aki, T. Endo, K. Sueyoshi, H. Hisamoto, Plasticized poly(vinyl chloride)-based photonic crystal for ion sensing, *Anal. Chem.* 86 (2014) 11986–11991.
- [41] T. Endo, S. Ozawa, N. Okuda, Y. Yanagida, S. Tanaka, Reflectometric detection of influenza virus in human saliva using nanoimprint lithography-based flexible two-dimensional photonic crystal biosensor, *Sens. Actuators B* 148 (2010) 269–276.
- [42] W. Hashimoto, T. Endo, K. Sueyoshi, H. Hisamoto, Development of novel protease assay device using a nanoimprinted two-dimensional photonic crystal, *Chem. Lett.* 43 (2014) 1728–1730.
- [43] K. Aono, S. Aki, K. Sueyoshi, H. Hisamoto, T. Endo, Development of optical biosensor based on photonic crystal made of TiO<sub>2</sub> using liquid phase deposition, *Jpn. J. Appl. Phys.* 55 (2016).
- [44] T. Endo, C. Ueda, H. Kajita, N. Okuda, S. Tanaka, H. Hisamoto, Enhancement of the fluorescence intensity of DNA intercalators using nano-imprinted 2-dimensional photonic crystal, *Microchim. Acta* 180 (2013) 929–934.
- [45] K. Maeno, S. Aki, K. Sueyoshi, H. Hisamoto, T. Endo, Polymer-based photonic crystal cavity sensor for optical detection in the visible wavelength region, *Anal. Sci.* 32 (2016) 117–120.
- [46] T. Endo, M. Sato, H. Kajita, N. Okuda, S. Tanaka, H. Hisamoto, Printed two-dimensional photonic crystals for single-step label-free biosensing of insulin under wet conditions, *Lab Chip* 12 (2012) 1995–1999.
- [47] Y. Terada, W. Hashimoto, T. Endo, H. Seto, T. Murakami, H. Hisamoto, Y. Hoshino, Y. Miura, Signal amplified two-dimensional photonic crystal biosensor immobilized with glyco-nanoparticles, *J. Mater. Chem. B* 2 (2014) 3324–3332.
- [48] J. Sun, K. Maeno, S. Aki, K. Sueyoshi, H. Hisamoto, T. Endo, Design and fabrication of a visible-light-compatible, polymer-based photonic crystal resonator and waveguide for sensing applications, *Micromachines* 9 (2018) 410.
- [49] K. Nishiguchi, K. Sueyoshi, H. Hisamoto, T. Endo, Fabrication of gold-deposited plasmonic crystal based on nanoimprint lithography for label-free biosensing application, *Jpn. J. Appl. Phys.* 55 (2016) 08RE02.
- [50] D. Kawasaki, H. Yamada, K. Maeno, K. Sueyoshi, H. Hisamoto, T. Endo, Core-shell structured gold nanocone array for label-free DNA sensing, *ACS Appl. Nano Mater.* (2019) Accepted.
- [51] L.J. Guo, Nanoimprint lithography: methods and material requirements, *Adv. Mater.* 19 (2007) 495–513.
- [52] T. Endo, K. Keman, N. Nagatani, Y. Takamura, E. Tamiya, Label-free detection of peptide nucleic acid-DNA hybridization using localized surface plasmon resonance based optical biosensor, *Anal. Chem.* 77 (2005) 6976–6984.
- [53] Z. Gao, A. Agarwal, A.D. Trigg, N. Singh, C. Fang, C. Tung, Y. Fan, K.D. Buddharaju, J. Kong, Silicon nanowire arrays for label-free detection of DNA, *Anal. Chem.* 79 (2007) 3291–3297.